



Solid Aluminum Borohydrides for Prospective Hydrogen Storage

Iurii Dovgaliuk,^[a, b] Damir A. Safin,^[a] Nikolay A. Tumanov,^[a] Fabrice Morelle,^[a] Adel Moulai,^[a] Radovan Černý,^[c] Zbigniew Łodziana,^[d] Michel Devillers,^[a] and Yaroslav Filinchuk^{*[a]}

Metal borohydrides are intensively researched as high-capacity hydrogen storage materials. Aluminum is a cheap, light, and abundant element and Al^{3+} can serve as a template for reversible dehydrogenation. However, $\text{Al}(\text{BH}_4)_3$, containing 16.9 wt% of hydrogen, has a low boiling point, is explosive on air and has poor storage stability. A new family of mixed-cation borohydrides $\text{M}[\text{Al}(\text{BH}_4)_4]$, which are all solid under ambient conditions, show diverse thermal decomposition behaviors: $\text{Al}(\text{BH}_4)_3$ is released for $\text{M}=\text{Li}^+$ or Na^+ , whereas heavier derivatives evolve hydrogen and diborane. $\text{NH}_4[\text{Al}(\text{BH}_4)_4]$, containing both

protic and hydridic hydrogen, has the lowest decomposition temperature of 35 °C and yields $\text{Al}(\text{BH}_4)_3\cdot\text{NHBH}$ and hydrogen. The decomposition temperatures, correlated with the cations' ionic potential, show that $\text{M}[\text{Al}(\text{BH}_4)_4]$ species are in the most practical stability window. This family of solids, with convenient and versatile properties, puts aluminum borohydride chemistry in the mainstream of hydrogen storage research, for example, for the development of reactive hydride composites with increased hydrogen content.

Introduction

Metal borohydrides and their derivatives are of great interest as materials for energy storage due to their high hydrogen contents.^[1] Most alkali and alkaline-earth metal borohydrides match the recently revised the United States Department of Energy system targets for gravimetric and volumetric hydrogen capacities of 7.5 wt% and 70 g L^{-1} , respectively.^[2] However, simple metal borohydrides show high stability to pyrolysis; for example, LiBH_4 desorbs hydrogen at around 470 °C, and $\text{Mg}(\text{BH}_4)_2$ between 290 and 500 °C.^[3,4] The decomposition temperature can be tuned and significantly decreased in mixed-metal borohydrides by using the correlation between the decomposition temperature and the Pauling electronegativity of the metal cations.^[5–7] The underlying principle is the weakening of the B–H bonds in the borohydride with increased covalency of the $\text{M}\cdots\text{H}(\text{B})$ interaction. The destabilization of the

latter improves thermal decomposition properties of mixed-metal complex hydrides, making some of them suitable for the temperature range of operational fuel cells, 60–120 °C.^[8] This includes bimetallic Al-based borohydrides stabilized by chloride substitution,^[9,10] as well as Zn- and Cd-based borohydrides stabilized by alkali metals.^[11,12]

The favorable decomposition temperatures entail a different problem: metal borohydrides decomposing below 200 °C yield diborane B_2H_6 ,^[13] besides hydrogen, preventing full reversibility of these hydrogen storage systems. One of the known ways to overcome this problem is by utilizing reactive hydride composites (RHCs): a chemical reaction between two or more hydrides. The reaction products from the mixture of hydrides are different from those released by the individual constituents. Remarkably, the gravimetric hydrogen storage capacity remains as high as the hydrogen storage capacity of the individual hydrides, but the release of the side products, like diborane, can be significantly suppressed. One of the most successful examples of reversible hydrogen storage in the form of complex hydrides is found on addition of MgH_2 to lithium borohydride.^[14] The formation of MgB_2 in this system provides destabilization of LiBH_4 , lowering the hydrogen desorption temperature. There is great interest in finding new H-rich complex hydrides with low decomposition temperatures, especially those with cheap and abundant elements like Al.

Indeed, Al-containing hydrides and composites have attracted a great deal of attention as hydrogen storage media. In particular, alane AlH_3 ^[15] and alanates of alkali and alkaline-earth metals $\text{M}(\text{AlH}_4)_n$ ^[16] as well as Al–N–B-based hydrides^[17] are being intensively investigated. Among such species, NaAlH_4 is the most studied alanate, owing to its high hydrogen content of 5.6 wt% and the Ti-catalyzed reversible desorption and absorp-

[a] Dr. I. Dovgaliuk, Dr. D. A. Safin, Dr. N. A. Tumanov, F. Morelle, A. Moulai, Prof. M. Devillers, Prof. Y. Filinchuk
Institute of Condensed Matter and Nanosciences
Université catholique de Louvain
Place L. Pasteur 1, 1348 Louvain-la-Neuve (Belgium)
E-mail: yaroslav.filinchuk@uclouvain.be

[b] Dr. I. Dovgaliuk
Swiss-Norwegian Beamlines
European Synchrotron Radiation Facility
Martyrs, 38042 Grenoble Cedex 9 (France)

[c] Prof. R. Černý
Laboratory of Crystallography, DQMP, University of Geneva
quai Ernest-Ansermet 24, 1211 Geneva (Switzerland)

[d] Prof. Z. Łodziana
Department of Structural Research, INP Polish Academy of Sciences
ul. Radzikowskiego 152, 31-342 Kraków (Poland)

Supporting Information and the ORCID identification number(s) for the author(s) of this article can be found under <https://doi.org/10.1002/cssc.201701629>.

tion of hydrogen.^[18] The following studies demonstrate reversible hydrogen cycling over 100 cycles with a measured capacity of about 4 wt% at 160 °C.^[19] Some Al-based RHCs are also known, such as LiBH₄–LiH–Al, which reabsorbs 5.1 wt% of hydrogen at 350 °C under a pressure of 70 bar.^[20] For another Al-containing composite, namely LiBH₄–MgH₂–Al, the dehydrogenation onset temperature is 100 °C lower than that of the starting Al-free LiBH₄–MgH₂ composite.^[21,22] Hence, the addition of Al improves some RHCs by lowering their operating temperatures.

Recently, it was shown that the highly polarizing Al³⁺ significantly alters the properties of complex and chemical hydrides, such as borohydrides or ammonia borane.^[17] Effectively, Al³⁺ is a strong Lewis acid that can serve as a template in chemical transformations of hydrides. Aluminum is capable of coordinating both the initial hydrogenated species as well as the dehydrogenation products,^[23] enabling in some cases a hydrogen desorption reversibility.

Despite numerous studies having been devoted to the chemistry of boron and aluminum hydrides, neither borohydrides of Al nor their RHCs have to date been well explored. This deficiency arises from difficulties in handling the highly pyrophoric and explosive liquid aluminum borohydride, making Al(BH₄)₃ highly inconvenient in experimental work, owing to its fast decomposition.^[24] Thus, Al(BH₄)₃ stabilized in a solid form as [Al(BH₄)₄][−] anions^[25] can serve as a platform either for safe Al(BH₄)₃ storage, as it recently proposed by Popczun et al.,^[26] or for the design of novel RHCs. This beneficial feature can be used not only for hydrogen storage, but also in technological processes such as the fabrication of the light-emitting wide-gap Al_{1−x}B_x semiconductor technologies (e.g., Al_{1−x}B_xPSi₃),^[27] as well as a prospective green bipropellant rocket fuel.^[28]

Herein, we report on the synthesis, crystal structures, thermal analysis, and Raman and NMR spectroscopy studies, together with the detailed DFT calculations of a series of Al(BH₄)₃-based mixed-cation borohydrides, M[Al(BH₄)₄] (M = Li⁺, Na⁺, K⁺, NH₄⁺, Rb⁺, Cs⁺). We show that the members of the series decompose between 35 and 150 °C, yielding a variety of products, including Al(BH₄)₃, H₂, and B₂H₆. The stability of the new series is related to the ionic potential of metal atoms and is favorable compared to other known metal borohydrides. The thermodynamic assessment of the RHCs using M[Al(BH₄)₄] with light metal hydrides suggests potentially reversible hydrogen storage in these systems.

Results and Discussion

All mixed-cation borohydrides were obtained by the addition reaction of Al(BH₄)₃ and MBH₄ (M = Li⁺, Na⁺, K⁺, NH₄⁺, Rb⁺, Cs⁺). NH₄[Al(BH₄)₄] was produced with an almost quantitative yield of 97.3(9) wt%, whereas the alkali metal borohydrides had to be ground and soaked in Al(BH₄)₃ two to four times to reach high yields. The fact that several milling/soaking cycles are required can be explained by the formation of M[Al(BH₄)₄] on the surface of MBH₄, which prevents completion of the reaction. Below we briefly describe the interaction of Al(BH₄)₃

with MBH₄, products of their decomposition and the crystal structures of the obtained phases and evaluate the stability of the Al-based borohydride series with respect to other known borohydrides.

Formation and thermal stability of the mixed-cation aluminum borohydrides

Synchrotron powder X-ray diffraction (PXRD) was used to reveal the whole series of the mixed-cation M[Al(BH₄)₄] structures (M = Li⁺, Na⁺, K⁺, NH₄⁺, Rb⁺, Cs⁺). The diffraction data were used to solve the crystal structures (see below) and variable-temperature diffraction studies allowed to characterize their thermal decomposition (Figure 1 and Figures S1–S3 in the

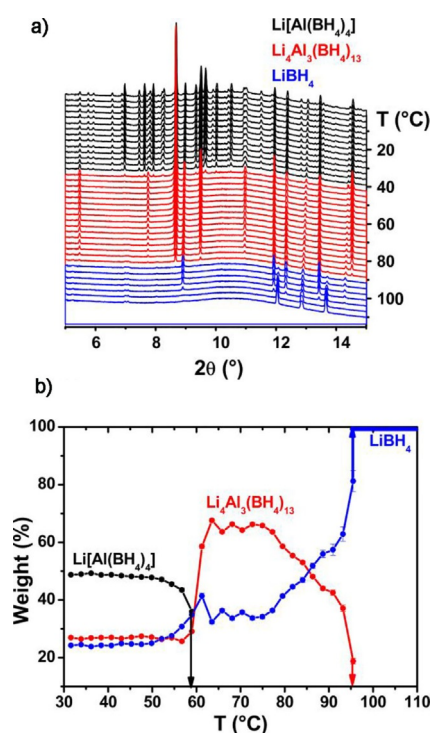
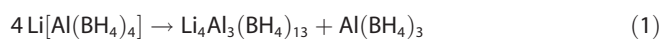
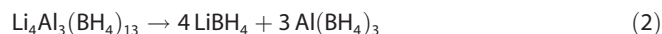


Figure 1. a) The plot of the variable temperature in situ powder patterns of Li[Al(BH₄)₄], Li₄Al₃(BH₄)₁₃, and LiBH₄. b) The mass fractions extracted from the Rietveld refinement on in situ PXRD patterns (Materials Science Beamline, PSI, Mythen II detector, $\lambda = 0.775045$ Å).

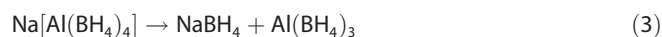
Supporting Information). The reaction with LiBH₄ produces two different mixed-metal complexes, Li[Al(BH₄)₄] and Li₄Al₃(BH₄)₁₃ (Figure 1). To our knowledge, Li[Al(BH₄)₄] was not previously known, whereas Li₄Al₃(BH₄)₁₃ was found to be isostructural to the Cl-substituted Li₄Al₃(BH₄)_{12.74}Cl_{0.26} obtained by ball milling AlCl₃ with LiBH₄.^[9] Li₄Al₃(BH₄)₁₃ is more stable at room temperature and the diffraction peaks of Li[Al(BH₄)₄] gradually decrease on heating and completely vanish at about 60 °C (Figure 1). The amount of Li₄Al₃(BH₄)₁₃ abruptly increases at the same temperature, thus Equation (1) be derived:



Note that the boiling point of $\text{Al}(\text{BH}_4)_3$ is 44°C and thus it can not be observed by diffraction. The complementary measurements by thermogravimetric analysis (TGA) and differential scanning calorimetry (DSC) in the range of $50\text{--}90^\circ\text{C}$ exhibit one endothermic decomposition step with a maximum at 89°C (Figure S4, top). Thus, $\text{Li}_4\text{Al}_3(\text{BH}_4)_{13}$ is a major phase at $60\text{--}80^\circ\text{C}$, but it completely decomposes at about 90°C , releasing $\text{Al}(\text{BH}_4)_3$ and LiBH_4 according to a known reaction [Equation (2)].^[25b]



In situ diffraction shows that the heavier $\text{M}[\text{Al}(\text{BH}_4)_4]$ species decompose at slightly higher temperatures: at 90°C for $\text{M}=\text{Na}$ (Figure S1), at 160°C for $\text{M}=\text{K}$ ^[26,29] and Rb (Figure S2), and at around 150°C for $\text{M}=\text{Cs}$ (Figure S3). According to TGA and DSC (Figure S4), $\text{Na}[\text{Al}(\text{BH}_4)_4]$ decomposes at $70\text{--}110^\circ\text{C}$, with a mass loss corresponding to the extraction of the volatile aluminum borohydride. Considering the formation of NaBH_4 detected by PXRD, Equation (3) can be derived:



Contrary to the lighter $\text{M}[\text{Al}(\text{BH}_4)_4]$ species ($\text{M}=\text{Li}^+$, Na^+ , K^+), which form the corresponding crystalline MBH_4 , the intensities of RbBH_4 and CsBH_4 increase insignificantly upon decomposition of the Al-based hydride. The increased background upon the thermal decomposition of high-temperature $\text{HT-Cs}[\text{Al}(\text{BH}_4)_4]$ at around 150°C indicates the formation of amorphous product(s), while some amount of the cubic CsBH_4 forms only upon further heating above 165°C . The TGA plots for $\text{Rb}[\text{Al}(\text{BH}_4)_4]$ and $\text{Cs}[\text{Al}(\text{BH}_4)_4]$ contain two poorly defined decomposition steps with total weight losses of 13.2 and 4.5%, respectively (Figure S5). These values are significantly lower than 41.6 and 32.6 wt% expected for the release of volatile $\text{Al}(\text{BH}_4)_3$. Nevertheless, the weight loss for $\text{Rb}[\text{Al}(\text{BH}_4)_4]$ is higher than the calculated hydrogen content of 9.4 wt%, suggesting a release of heavier gases. Indeed, according to the TGA-MS and volumetric data, the first decomposition step of $\text{Rb}[\text{Al}(\text{BH}_4)_4]$ is accompanied by the release of hydrogen and diborane, whereas only hydrogen is detected during the second decomposition step (giving 4 mol of gas in total per mol of $\text{Rb}[\text{Al}(\text{BH}_4)_4]$; see Figures S6 and S7). In contrast, the total weight loss by $\text{Cs}[\text{Al}(\text{BH}_4)_4]$ of 4.5% is smaller than the calculated hydrogen content of roughly 7.4 wt% (4.5 mol of gas in total; see Figure S7). This might be an indication of the release of pure hydrogen upon thermal decomposition. However, TGA-MS and volumetric data show the simultaneous release of hydrogen and diborane during the first decomposition step (Figures S7 and S8 in the Supporting Information), and the release of hydrogen only during the second step, similar to the behavior of the Rb-containing analogue. Interestingly, the previous theoretical investigations of $\text{Rb}[\text{Al}(\text{BH}_4)_4]$ and $\text{Cs}[\text{Al}(\text{BH}_4)_4]$ clusters suggested their higher stability with respect to fragmentation into MBH_4 and $\text{Al}(\text{BH}_4)_3$, compared to $\text{K}[\text{Al}(\text{BH}_4)_4]$.^[26] This is in agreement with the present periodic calculations (see Figure 3). However, our experimental observations can be ex-

plained by the formation of different decomposition products from MBH_4 and $\text{Al}(\text{BH}_4)_3$.

$\text{NH}_4[\text{Al}(\text{BH}_4)_4]$ will be discussed separately, owing to its unique thermal decomposition behavior. It arises from the co-existence of protic H^+ and hydridic H^- , which form dihydrogen bonds in the structure that easily recombine even on slight heating. PXRD reveals the formation of nearly pure $\text{NH}_4[\text{Al}(\text{BH}_4)_4]$ (Figure S9). This compound is the most unstable within the series and melts with a decomposition at 35°C . It does not form the initial NH_4BH_4 upon decomposition, but a number of species related to the dehydrogenation of the mixed-cation borohydride as a whole.

TGA data on the sample containing approximately 97 wt% of the crystalline $\text{NH}_4[\text{Al}(\text{BH}_4)_4]$ reveal two clearly defined decomposition steps (Figure S10). The decomposition of the complex starts at about 35°C with a weight loss of about 13.6%, whereas the second decomposition step occurs at 58°C and with a roughly 20.5% weight loss. Similar two-step weight loss was also observed upon the thermal decomposition of $\text{Al}(\text{BH}_4)_3\cdot\text{NH}_3\text{BH}_3$.^[23] According to the TGA-MS data on $\text{NH}_4[\text{Al}(\text{BH}_4)_4]$, both decomposition steps are accompanied by the release of hydrogen, diborane, and ammonia (Figure S11). No detectable amounts of $\text{Al}(\text{BH}_4)_3$ were observed by mass spectrometry. Complementary volumetric studies, performed at the constant temperature of 40°C , revealed the release of about 3 mol of gas per mol of $\text{NH}_4[\text{Al}(\text{BH}_4)_4]$ (Figure S12) during the first decomposition step.

To clarify the nature of the decomposition products of $\text{NH}_4[\text{Al}(\text{BH}_4)_4]$, ^{11}B , $^{11}\text{B}\{^1\text{H}\}$, ^{27}Al , $^{27}\text{Al}\{^1\text{H}\}$, and ^1H NMR spectroscopy experiments were performed in $[\text{D}_8]$ toluene. The freshly dissolved sample was studied, as well as the toluene solutions aged at room temperature for 2 and 10 days. The assignment of signals is given in the Supporting Information. The main decomposition product is $\text{Al}(\text{BH}_4)_3\cdot\text{NHBH}$, previously identified as the main product of $\text{Al}(\text{BH}_4)_3\cdot\text{NH}_3\text{BH}_3$ dehydrogenation.^[23] In addition, there is a secondary reaction pathway leading to $\text{Al}(\text{BH}_4)_3$, slowly decomposing to $[\text{HAl}(\text{BH}_4)_2]$ and B_2H_6 . The MS measurements on the gases evolving from the solid $\text{NH}_4[\text{Al}(\text{BH}_4)_4]$ (Figure S10) show no $\text{Al}(\text{BH}_4)_3$, and, hence, this reaction path is characteristic for the solution in $[\text{D}_8]$ toluene. The main decomposition pathway both in toluene (as seen by NMR spectroscopy) and in solvent-free conditions (as seen by the volumetric and DSC/TGA-MS methods) can be described by the Equation (4):



Notably, neither NMR spectroscopy in solution nor the in situ PXRD on the crystalline $\text{NH}_4[\text{Al}(\text{BH}_4)_4]$ detect the formation of $\text{Al}(\text{BH}_4)_3\cdot\text{NH}_3\text{BH}_3$,^[23] expected as an intermediate by analogy with the perovskite type $\text{NH}_4\text{Ca}(\text{BH}_4)_3$, transforming into $\text{Ca}(\text{BH}_4)_2\cdot\text{NH}_3\text{BH}_3$.^[30,31]

To summarize on the formation and stability of the Al-based borohydrides, we conclude that the Li–Al and Na–Al borohydrides can be seen as convenient stores of aluminum borohydride, as they are stable at room temperature with no significant amount of polymerization to higher boranes typical for

$\text{Al}(\text{BH}_4)_3$.^[32] The latter can be obtained upon heating the bimetallic compounds to moderate temperatures (60–90 °C). The heavier $\text{M}[\text{Al}(\text{BH}_4)_4]$ species ($\text{M}=\text{K}^+, \text{Rb}^+, \text{Cs}^+$) irreversibly release hydrogen (no readsorption even at $p(\text{H}_2)=100$ bar) and some improvements should be implemented for their practical application. In particular, we surmise the possibility of making the RHCs, as discussed below.

Crystal structures of the mixed-cation aluminum borohydrides

All of the crystal structures were determined from synchrotron powder diffraction data, and subsequently optimized by DFT methods (see the Experimental Section and the Supporting Information for details). $\text{Li}[\text{Al}(\text{BH}_4)_4]$ crystallizes in the monoclinic space group $P2_1/c$ with four independent cations and complex anions. All the Li^+ and Al^{3+} cations are surrounded by four BH_4^- anions, coordinated via edges (Figure 2). As a result of these interactions, a 3D framework constructed from distorted $[\text{Al}(\text{BH}_4)_4]^-$ “supertetrahedra” is formed, resembling the structure of LiBH_4 .^[33] The underlying net, as analyzed by the program TOPOS,^[34] is a 4-connected net of a new type containing four nodes (two Li^+ and two Al^{3+}) with the point symbol $\{4.6^2.8^3\}\{4.6^4.8\}$. The framework character of the compound is underlined by a similar distance between Li^+ and Al^{3+} from bridging BH_4^- when normalized to the sum of the ionic radii (cation + anion; see the Supporting Information for more details of the molecular geometry in the crystal structures).

$\text{Li}_4\text{Al}_3(\text{BH}_4)_{13}$ crystallizes in the cubic $P\bar{4}3n$ space group, with a structure identical to the previously reported $\text{Li}_4\text{Al}_3(\text{BH}_4)_{12.74}\text{Cl}_{0.26}$.^[8] The composition of these compounds can be rationalized on the basis of a complex cation $[(\text{BH}_4)\text{Li}_4]^{3+}$ and an anion $[\text{Al}(\text{BH}_4)_4]^-$, packed as in the Frank–Kasper Cr_3Si -type phase.^[8] Our topology analysis indicates that $[(\text{BH}_4)\text{Li}_4][\text{Al}(\text{BH}_4)_4]_3$ is an antitype of Ag_3PO_4 .^[35]

$\text{Na}[\text{Al}(\text{BH}_4)_4]$ crystallizes in the monoclinic space group $C2/c$. The Na^+ atom is in a distorted octahedral coordination environment formed by six BH_4^- groups coordinated via edges (Figure 2). This coordination is typical in other Na-containing borohydrides, for example, $\text{Na}[\text{Al}(\text{BH}_4)_{4-x}\text{Cl}_x]$ ^[10] and NaBH_4 .^[36] Importantly, $\text{Na}[\text{Al}(\text{BH}_4)_4]$ takes a different structure, with 90° reorientation of the complex anion with respect to the Na^+ counterions, than in the Cl-substituted phase.^[10] Its structure is a monoclinic deformation of $\text{Na}[\text{Sc}(\text{BH}_4)_4]$,^[37] which itself is of the CrVO_4 type. Each $[\text{Na}(\text{BH}_4)_6]^{5+}$ octahedron in the structure of $\text{Na}[\text{Al}(\text{BH}_4)_4]$ is linked via edges to the neighboring octahedra, producing layers that in turn are linked by vertices to the tetrahedral $[\text{Al}(\text{BH}_4)_4]^-$ anions (Figure 2).

The crystal structure of $\text{K}[\text{Al}(\text{BH}_4)_4]$ was reported earlier in the space group $Fddd$ ^[29] and in its subgroup $Fdd2$.^[26] We have made the normal mode analysis for the $Fdd2$ structure and found that the structure is stable with respect to atomic displacements. However, the simulated annealing procedure applied to this phase resulted in the stable $Fddd$ symmetry (Table S1 in the Supporting Information). The ground-state electronic energy and the zero-point energy of the structure

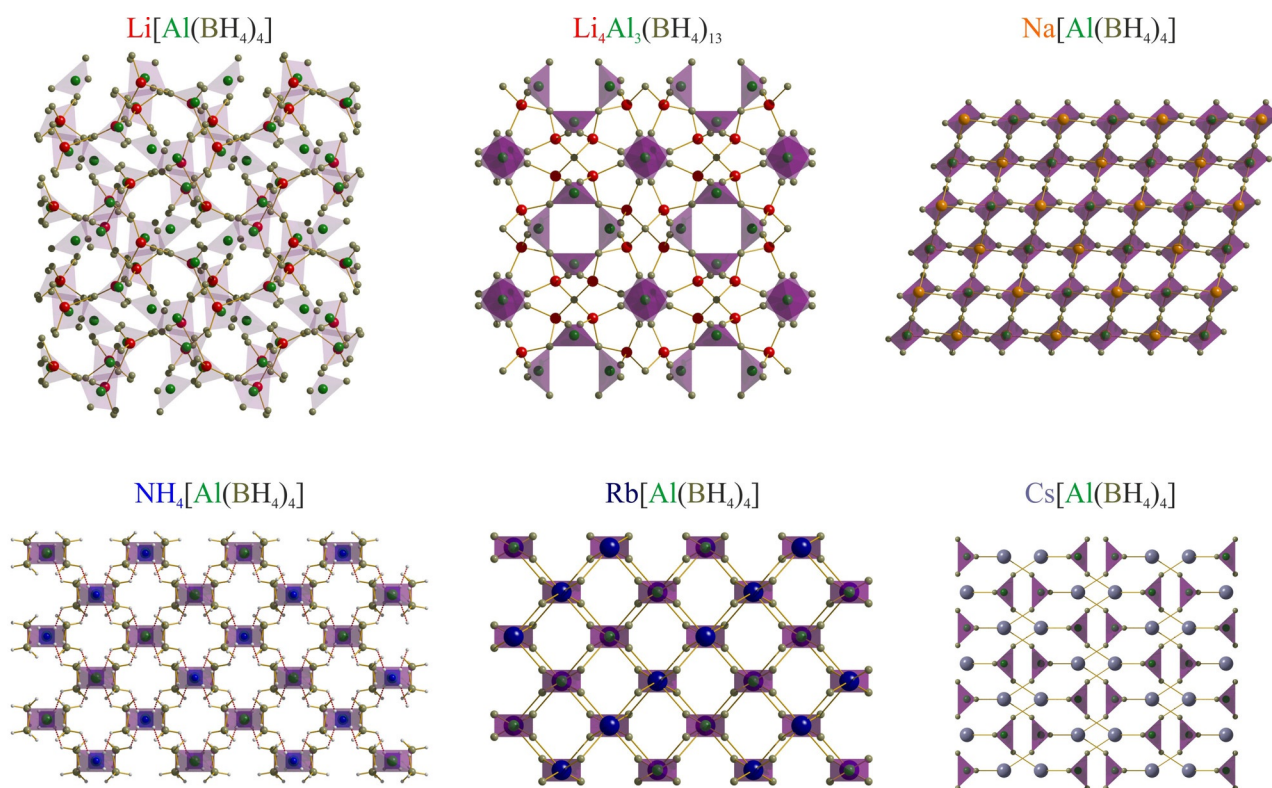


Figure 2. Crystal packing of the mixed-cation aluminum borohydride frameworks along the a ($\text{Li}[\text{Al}(\text{BH}_4)_4]$) and b axes. The complex $[\text{Al}(\text{BH}_4)_4]^-$ anions are represented as flattened purple “supertetrahedra” and H atoms are omitted for clarity (except those in $\text{NH}_4^+[\text{Al}(\text{BH}_4)_4]$, which contains red dihydrogen bonds between BH_4^- and NH_4^+ ions). Color code: Al = green, B = olive, H = gray, Li = red, Na = orange, N = blue, Rb = blue dark, Cs = blue gray.

with the *Fddd* symmetry are equal to within 1 meV per formula unit (f.u.) of those for the *Fdd2* one. Therefore, we can confirm the higher space group symmetry *Fddd* for $K[Al(BH_4)_4]$.^[29] In that study, we found that $NH_4[Al(BH_4)_4]$ and $Rb[Al(BH_4)_4]$ are isomorphous to the K-containing analogue with the *Fddd* structure.^[29] An important difference for the former case is the presence of the short dihydrogen (N)H⁺...H⁻(B) bonds (Figure 2). The experimental H...H distance of 1.82 Å is confirmed by the DFT calculations (Table S1 in the Supporting Information) and found to be significantly shorter than those in NH_3BH_3 (1.91(5) Å)^[38] and in NH_4BH_4 (2.28 Å).^[39]

The high-temperature polymorph of $Cs[Al(BH_4)_4]$ crystallizes in the tetragonal space group *I4₁/amd*. Its crystal structure is derived from the scheelite type,^[40] which is also the prototype of another mixed-cation borohydride $Cs[Y(BH_4)_4]$.^[41] The powder pattern of the room-temperature polymorph was indexed in a monoclinic unit cell, which points towards a structural relation known between scheelite and monazite.^[42] In spite of the significant efforts, no reliable structural model was obtained for the room-temperature polymorph. In the HT polymorph, the Cs⁺ cation coordinates (4 + 8) BH₄⁻ groups with Cs...B distances of 3.66(7) and 4.53(3) Å (Figure 2). The adjacent coordination polyhedra share pseudo-square faces (4.01 × 4.43 Å²), resulting in the formation of an infinite 3D framework.

Raman spectroscopy

The Raman spectra of $M[Al(BH_4)_4]$ ($M = Li^+, Na^+, NH_4^+, Rb^+, Cs^+$) all include bands for the B–H bending and stretching modes of the BH₄⁻ ligands in the $[Al(BH_4)_4]^-$ anion at 1000–1500 cm⁻¹ and 2100–2600 cm⁻¹, respectively (Figure S14 in the Supporting Information). The stretching mode bands are characteristic for the bidentate-coordinated borohydride anions.^[43] The same was observed in the Raman spectrum of $K[Al(BH_4)_4]$.^[29] The complex anion $[Al(BH_4)_4]^-$ is also visible in the Raman spectra, with a characteristic band at about 460 cm⁻¹ that arises from the Al...H–B stretching mode. Moreover, the Raman spectrum of $Na[Al(BH_4)_4]$ contains a characteristic band for $NaBH_4$, centered at about 2330 cm⁻¹. The spectrum of $Li[Al(BH_4)_4]$ is further complicated by the presence of bands for $LiBH_4$ and $Li_4Al_3(BH_4)_{13}$.

Formation energies

To delineate the thermodynamic parameters of the $M[Al(BH_4)_4]$ series for potential application in RHCs, the enthalpies of formation for the $M[Al(BH_4)_4]$ series and for $Li_4Al_3(BH_4)_{13}$ were calculated from the ground-state energies of the corresponding structures and of the starting $Al(BH_4)_3$ and MBH_4 (Figure 3). The *Pna2* structure was used for $Al(BH_4)_3$ as a reference.^[44] The low-temperature structures were used for MBH_4 , as described recently.^[45] The *P4₂/nmc* symmetry was applied for the MBH_4 ($M = Rb^+, Cs^+$) structures, whereas, according to our calculations, the lowest energy structure of NH_4BH_4 has the *P-42₁c* symmetry. However, the latter structure is unstable with respect to the orientation of NH_4^+ (imaginary modes related to

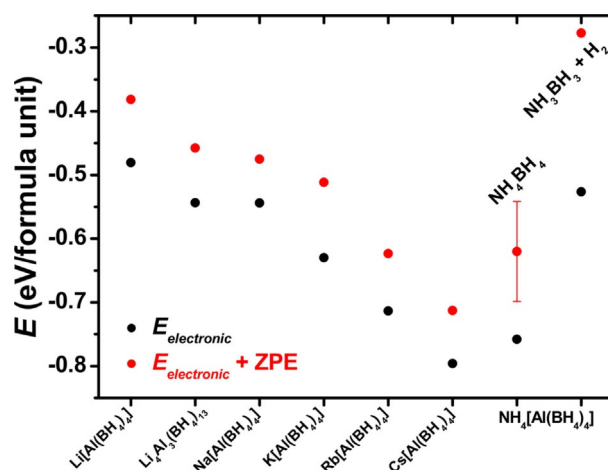


Figure 3. Calculated enthalpies of formation of mixed-cation borohydrides from one mole of $Al(BH_4)_3$ and the corresponding MBH_4 . Black circles are for the ground-state electronic energy and red circles account for the zero-point vibrations.

the NH_4^+ rotation), as well as to the decomposition into NH_3BH_3 and H_2 .^[46] Therefore, two sets of data, corresponding to the decomposition into disordered/unstable NH_4BH_4 and to decomposition into NH_3BH_3 and H_2 , are shown for $NH_4[Al(BH_4)_4]$ (Figure 3). The error bar accounts for four imaginary modes related to the NH_4^+ librations. The calculated enthalpies indicate that all compounds are stable with respect to decomposition into binary borohydrides, and this stability increases for heavier alkali metals. There is an additional decomposition path for $Li[Al(BH_4)_4]$ according to the Equation (1), with experimentally observed $Li_4Al_3(BH_4)_{13}$. The calculated electronic contribution to the enthalpy of this reaction is -0.29 eV per f.u. The zero-point vibrations increase this enthalpy up to -0.15 eV per f.u.

The reaction $NH_3BH_3 + H_2 \rightarrow NH_4BH_4$ is endothermic with a calculated $\Delta H = +0.15 \div 0.42$ eV per f.u., which is reflected in the lower stability of $NH_4[Al(BH_4)_4]$ compared to $NH_3BH_3 + H_2$ (Figure 3).

Composition–structure–stability relations

The first attempt to explain the stability of the Al-based series of borohydrides is based on the first Pauling's rule,^[47] stating in particular that the cation/anion radius ratio (r_C/r_A) determines the coordination number of the cation.

The Li^+ cation in $Li[Al(BH_4)_4]$ adopts a tetrahedral coordination environment by the BH_4^- groups, matching the stability window defined by the r_C/r_A ratio (Figure 4). Nevertheless, this compound exhibits relatively low thermal stability. The Na^+ cation in $Na[Al(BH_4)_4]$ has an octahedral environment by the BH_4^- groups, as expected for the given r_C/r_A ratio (Figure 4), and is more stable than its Li-based analogue. The K^+ , Rb^+ , and Cs^+ -containing derivatives have similar and relatively high stabilities (Figure 4). Their coordination numbers range from 4 + 4 to 4 + 8, being higher than the typical value of 6 in this r_C/r_A window. The $[(BH_4)Li_4]^{3+}$ is significantly larger than the other cations and falls into the stability region of icosahedral

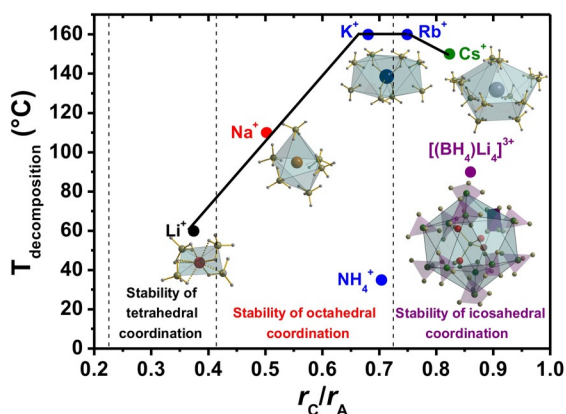


Figure 4. Thermal stabilities of $M[\text{Al}(\text{BH}_4)_4]$ species ($M = \text{Li}^+, \text{Na}^+, \text{K}^+, \text{NH}_4^+, \text{Rb}^+, \text{Cs}^+$) and of $[(\text{BH}_4)\text{Li}_4][\text{Al}(\text{BH}_4)_4]_3$ as a function of the cation/anion ratio. The dashed lines define the stability regions of the coordination polyhedra according to the first Pauling's rule. The observed coordination environments (colored circles: black = tetrahedral, red = octahedral, blue = 4 + 4, olive = 4 + 8, purple = icosahedral, the latter is based on the size ratio for the complex cation and the complex anion) do not fully match the stability regions. The observed mismatch does not explain the variation of the decomposition temperatures.

coordination, considering the much larger $[\text{Al}(\text{BH}_4)_4]^-$ anion. Indeed, this cation has the expected icosahedral coordination by the complex anions (Figure 4), but the stability of $[(\text{BH}_4)\text{Li}_4][\text{Al}(\text{BH}_4)_4]_3$ is much lower than for $M = \text{K}^+, \text{Rb}^+, \text{and } \text{Cs}^+$. The radius of the $[\text{Al}(\text{BH}_4)_4]^-$ anion was found, based on the crystal structure data of the described borohydrides, to be roughly 3 Å. $\text{NH}_4[\text{Al}(\text{BH}_4)_4]$ is a special case, as it has the same structure and r_c/r_A ratio as for $M = \text{K}^+$ or Rb^+ , but is much less stable, which is likely due to the formation of $(\text{N})\text{H}^{\delta+} \cdots \text{H}^{\delta-}(\text{B})$ dihydrogen bonds (Figure 2) that easily recombine into H_2 .

We can thus conclude that the observed coordination numbers do not match well the stability regions deduced from the geometrical principles of the first Pauling's rule. Moreover, the observed mismatches do not explain the variation of decomposition temperatures. Therefore, in the second attempt to address the structure–property relations, we had to take into account electronic factors.

The relation between the formation enthalpies of metal borohydrides (Figure 5) and the Pauling electronegativities^[5–7] has driven the idea of synthesis of mixed-cation borohydrides aiming to tune the decomposition temperature. This semi-empirical rule holds well for alkali metals, however deviation is observed for the compounds containing transition metals or metals with a higher oxidation state. Recently, it was shown that the ionic potential ($\varphi = Z^*/r$, where r is the ionic radius of a cation) provides a simple measure of the stability of mixed-cation borohydrides,^[45] as long as the Born effective charges are taken as the charge of cations. The Born effective charges measure polarization induced by the displacement of ions, thus they are sensitive to the nature of interatomic bonding within the crystal and to the site symmetry of ions.

We have calculated the Born effective charges for the members of the title series and matched them with the decomposition temperatures (Figure 5; decomposition temperatures of

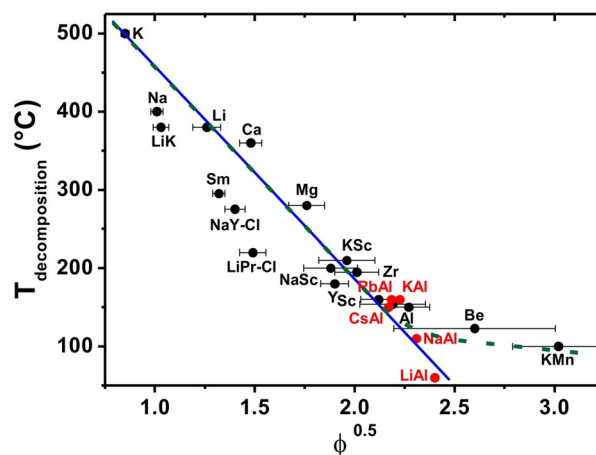


Figure 5. The experimental decomposition temperatures of metal borohydrides as a function of the ionic potential obtained by using the calculated dynamical charges on cations. The results of the present work are shown as red circles, whereas the data shown as black circles were taken from Ref. [45]. Highly polarized metal cations shift the linearity of the fitted curve (dashed green).

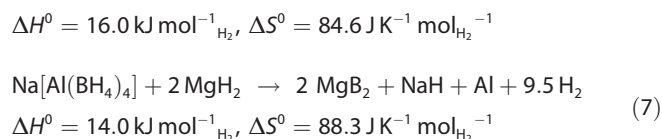
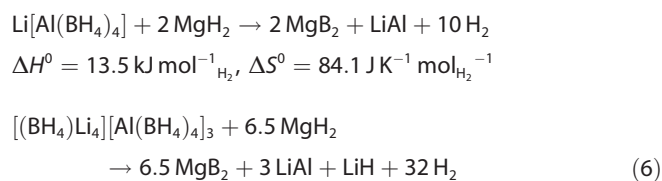
the new compounds reported herein are depicted in red, and those for the common metal borohydrides are in black). The data follow the linear regression of the decomposition temperature vs. the ionic potential. All of the Al-based borohydrides are located in the region of high ionic potentials with $\varphi^{0.5}$ higher than 2.

The Al-based bimetallic compounds combining even more strongly polarizing Mg^{2+} or Ca^{2+} cations would lead to decomposition at room temperature and thus are most likely unstable under ambient conditions. Indeed, our attempts to isolate bimetallic borohydrides in the $\text{Mg}(\text{BH}_4)_2\text{--Al}(\text{BH}_4)_3$ and $\text{Ca}(\text{BH}_4)_2\text{--Al}(\text{BH}_4)_3$ systems were unsuccessful. Consequently, the title family of Al-based borohydrides is complete in practical terms: any new members with higher ionic potential will be too unstable for application. Nevertheless, the diverse family presented herein, having convenient and versatile decomposition properties, puts aluminum borohydrides into mainstream research in hydrogen storage, for example, for the development of reactive hydride composites with increased hydrogen content.

Thermodynamic evaluation of mixed-cation aluminum borohydrides in RHCs

The optimal stability, versatility of the decomposition reaction pathways, low cost of raw materials, and exceptional hydrogen storage densities make these compounds highly interesting for the design of new reactive hydride composites involving metal hydrides, such as MgH_2 or CaH_2 .^[48] The thermodynamic evaluation was done by using the calculated formation enthalpies for the Al-based series from the corresponding monometallic borohydrides (Figure 3), omitting the formation entropy term, the formation energy of LiAl at 415°C ^[49] and the thermodynamic data for MgB_2 from Ref. [50]. The thermodynamics of possible decomposition pathways [Equations (5)–(7)] indicate that all

the reactions are endothermic and can potentially be rendered reversible by applying hydrogen pressure:



The estimated hydrogen pressure required for rehydrogenation at 295 °C is 100 bar for Equation (5), 39 bar for Equation (6) and 136 bar for Equation (7).

The synthesis of $\text{M}[\text{Al}(\text{BH}_4)_4]$ precursors can be scaled up by using mechanochemical methods, making the synthesis also much cheaper. Remarkably, ball milling of AlCl_3 with MBH_4 yields the lighter members of the series^[9,10] with still high hydrogen capacity in the resulting mixtures, for example, 7.7 wt% for $[(\text{BH}_4)\text{Li}_4][\text{Al}(\text{BH}_4)_3] + \text{LiCl}$, compared to 17.2 wt% for pure $[(\text{BH}_4)\text{Li}_4][\text{Al}(\text{BH}_4)_3]$. The thermodynamically feasible between the ball-milled $[(\text{BH}_4)\text{Li}_4][\text{Al}(\text{BH}_4)_3]$ and LiCl or $\text{Na}[\text{Al}(\text{BH}_4)_4-x\text{Cl}_x] + \text{NaCl}$ with MgH_2 [Equations (6) and (7)] do not occur either at room temperature or upon heating. The thermal decomposition of $[(\text{BH}_4)\text{Li}_4][\text{Al}(\text{BH}_4)_3]$ and $\text{Na}[\text{Al}(\text{BH}_4)_4-x\text{Cl}_x]$ starts at lower temperatures than Equations (6) and (7) (see Figures S15 and S16). The use of hydrogen back-pressure may make this behavior more favourable, thus more attempts should be made, also using more reactive alkali metal hydrides.

Conclusions

A new family of Al-based hydrogen-rich borohydrides $\text{M}[\text{Al}(\text{BH}_4)_4]$ ($\text{M} = \text{Li}^+, \text{Na}^+, \text{K}^+, \text{NH}_4^+, \text{Rb}^+, \text{Cs}^+$) was obtained by the reaction of solid MBH_4 with liquid $\text{Al}(\text{BH}_4)_3$. The thermal decomposition properties of $\text{M}[\text{Al}(\text{BH}_4)_4]$ are diverse: $\text{Al}(\text{BH}_4)_3$ is released below 100 °C for $\text{M} = \text{Li}^+$ and Na^+ , whereas heavier derivatives evolve hydrogen and diborane at about 150 °C. $\text{NH}_4[\text{Al}(\text{BH}_4)_4]$ represents a special case, as it contains protic and hydridic hydrogen, recombining into hydrogen already at 35 °C. Its major decomposition product is $\text{Al}(\text{BH}_4)_3 \cdot \text{NHBH}$, which was recently observed upon thermal decomposition of $\text{Al}(\text{BH}_4)_3 \cdot \text{NH}_3\text{BH}_3$.^[23] $\text{M}[\text{Al}(\text{BH}_4)_4]$ can be seen as a convenient store of the highly unstable aluminum borohydride, as well as extremely H-rich substances suitable for the design of new hydrogen (energy) storage materials. With its diverse, convenient, and versatile decomposition properties, the aluminum borohydrides should enter mainstream research in hydrogen storage, for example, for the development of reactive hydride composites with increased hydrogen content.

Experimental Section

Materials and analytical methods

All reactions were performed using commercially available reagents: AlCl_3 , LiBH_4 , NaBH_4 (from Sigma Aldrich with > 95 % purity), LiBH_4 (from Boss chemical industry Co., China with 96% purity), RbBH_4 , CsBH_4 (from Katchem), NH_4F (from Sigma Aldrich with 98.8% purity) and anhydrous NH_3 (from Praxair).

Raman spectroscopy: Spectra were recorded at room temperature with a Bruker RFS 100 s⁻¹ FT-Raman spectrometer ($I = 200 \text{ mW}$) in the 100–4000 cm^{-1} range, using a diode-pumped, air-cooled Nd:YAG laser with 1064 nm excitation.

NMR spectroscopy: NMR spectra in $[\text{D}_8]\text{toluene}$ were collected on a Bruker Avance DRX500 spectrometer operating at 500.13 for ^1H , 160.461 MHz for ^{11}B and 130.318 MHz for ^{27}Al nuclei. Chemical shifts are reported with reference to SiMe_4 (TMS) for ^1H , $\text{BF}_3 \cdot \text{OEt}_2$ for ^{11}B and 1.1 M of $\text{Al}(\text{NO}_3)_3$ in D_2O for ^{27}Al .

Thermal analysis: Thermogravimetric analysis (TGA) and differential scanning calorimetry (DSC) were performed on powder samples. TGA of $\text{M}[\text{Al}(\text{BH}_4)_4]$ ($\text{M} = \text{Li}^+, \text{Na}^+$) was performed by using a PerkinElmer STA 6000 apparatus. The samples (ca. 2 mg) were loaded into an Al_2O_3 crucible and heated from room temperature to 400 °C (5 °C min⁻¹ heating rate) in a dynamic argon flow of 20 mL min⁻¹. $\text{NH}_4[\text{Al}(\text{BH}_4)_4]$ was measured on a TGA/DTA 851 Mettler instrument (1 °C min⁻¹ heating rate) from 25 to 150 °C with a dynamic nitrogen flow of 100 mL min⁻¹. All samples for thermal analysis were loaded in an argon-filled glove box.

Volumetric analysis and reversibility tests: Volumetric analysis was performed by using a Hiden Isochema IMI-SHP analyzer. $\text{NH}_4[\text{Al}(\text{BH}_4)_4]$ (ca. 40 mg) was heated from 30 to 40 °C (1 °C min⁻¹, $p(\text{He}) = 1 \text{ bar}$) and kept at this temperature for roughly 2 weeks. $\text{M}[\text{Al}(\text{BH}_4)_4]$ ($\text{M} = \text{Rb}^+, \text{Cs}^+$) was heated from 30 to 160 °C (5 °C min⁻¹, $p(\text{He}) = 1 \text{ bar}$). Subsequently, the gas release for all experiments was calculated from the calibrated volumes of the system, excluding the volume of the glass wool (2.06 g cm^{-3} density) and samples' skeletal volumes taken from their crystal structures. The rehydrogenation of remaining solid residues were performed by applying $p(\text{H}_2) = 100 \text{ bar}$ at 40 °C for $\text{NH}_4[\text{Al}(\text{BH}_4)_4]$ and 160 °C for $\text{M}[\text{Al}(\text{BH}_4)_4]$ ($\text{M} = \text{Rb}^+, \text{Cs}^+$), respectively.

Syntheses

$\text{Al}(\text{BH}_4)_3$: Caution! $\text{Al}(\text{BH}_4)_3$, which was synthesized as recently described,^[29] is a highly pyrophoric liquid that explodes on contact with air. All manipulations were carried out in a dedicated nitrogen-filled Plexiglas dry box.

NH_4BH_4 : Ammonium borohydride was synthesized by a slightly modified procedure^[51] by a metathesis reaction between ammonium fluoride and sodium borohydride in liquid ammonia ($\text{NaBH}_4 + \text{NH}_4\text{F} \rightarrow \text{NH}_4\text{BH}_4 + \text{NaF}$). Stoichiometric amounts of ammonium fluoride and sodium borohydride were weighed in the argon-filled glove box and loaded together with a magnetic stirrer into a round bottom flask (no. 1) equipped with a glass filter. The flask was connected to a Schlenk line and kept under a slight argon overpressure to avoid moisture contamination. Ammonia gas was first condensed at -78 °C by using a cold-finger condenser filled with dry ice and acetone, in a Schlenk flask (no. 2), containing a small amount of sodium metal to ensure complete dryness. When

the desired amount of liquefied ammonia (100 mL) was obtained, the ammonia bottle was disconnected and the condenser was replaced on flask no. 1, thus dry ammonia evaporated from flask no. 2 and was recondensed into flask no. 1. Once the ammonia transfer was complete, the reaction was left while stirring at reflux for 1 h. Then the solution was filtered to remove precipitated sodium fluoride and the solvent was removed under reduced pressure. The resulting product was transferred to the argon-filled glove box and kept in the freezer at -35°C . Given the high instability of ammonium borohydride, one of the main challenges of this synthetic procedure is to keep the product at a low temperature during synthesis and transfer from the Schlenk line to the storage freezer.

$M[\text{Al}(\text{BH}_4)_4]$ ($M = \text{Li}^+, \text{Na}^+, \text{K}^+, \text{NH}_4^+, \text{Rb}^+, \text{Cs}^+$): $\text{K}[\text{Al}(\text{BH}_4)_4]$ was prepared according to a recently described procedure.^[29] Other mixed-cation borohydrides were obtained in a manner similar to the potassium-containing analogue, according to the following reaction: $\text{Al}(\text{BH}_4)_3 + \text{MBH}_4 \rightarrow \text{M}[\text{Al}(\text{BH}_4)_4]$. Freshly prepared $\text{Al}(\text{BH}_4)_3$ (1–4 mL) was transferred by syringe into the flask, containing ground powders of MBH_4 (100–200 mg, $M = \text{Li}^+, \text{Na}^+, \text{NH}_4^+, \text{Rb}^+, \text{Cs}^+$) and stirred for 4–7 days. The reaction with NH_4BH_4 was carried out at -35°C in the glovebox freezer. The excess of volatile $\text{Al}(\text{BH}_4)_3$ was removed under vacuum. According to powder diffraction X-ray (PXRD), the yield of $\text{NH}_4[\text{Al}(\text{BH}_4)_4]$ was already 97.3(9) wt% after the first soaking cycle, owing to the high reactivity of ammonium borohydrides and partly to the low temperature preventing decomposition of the final product. However, for MBH_4 ($M = \text{Na}^+, \text{Rb}^+, \text{Cs}^+$), the first cycle of soaking in $\text{Al}(\text{BH}_4)_3$ yielded mixtures of $M[\text{Al}(\text{BH}_4)_4]$ and MBH_4 in about 1:1 weight ratio. The yield of the targeted products was significantly increased, up to ≈ 90 wt%, after the second soaking of the well-ground mixtures of $M[\text{Al}(\text{BH}_4)_4]/\text{MBH}_4$ in $\text{Al}(\text{BH}_4)_3$. The formation of $\text{Li}[\text{Al}(\text{BH}_4)_4]$ is always accompanied by $\text{Li}_4\text{Al}_3(\text{BH}_4)_{12.74}\text{Cl}_{0.26}$ and four cycles were required to obtain approximately 85 wt% yield. Lighter $M[\text{Al}(\text{BH}_4)_4]$ species ($M = \text{Li}^+, \text{Na}^+, \text{NH}_4^+$) are unstable at room temperature and should be stored in the fridge (typically at -35°C). Attention must be paid when washing the glassware after synthesis of lighter $M[\text{Al}(\text{BH}_4)_4]$ ($M = \text{Li}^+, \text{Na}^+, \text{NH}_4^+$), as the traces of their powders react vigorously with water. The alcohol should be used first.

Mechanochemical preparation of $\text{Li}_4\text{Al}_3(\text{BH}_4)_{12.74}\text{Cl}_{0.26}$, $\text{Na}[\text{Al}(\text{BH}_4)_{4-x}\text{Cl}_x]$ and their MgH_2 reactive hydrides composites: The chlorine-containing analogues of $[(\text{BH}_4)\text{Li}_4][\text{Al}(\text{BH}_4)_4]_3$ and $\text{Na}[\text{Al}(\text{BH}_4)_4]$ were prepared by previously described mechanochemical procedures.^[9,10] The formation of $\text{Li}_4\text{Al}_3(\text{BH}_4)_{12.74}\text{Cl}_{0.26}$ and $\text{Na}[\text{Al}(\text{BH}_4)_{4-x}\text{Cl}_x]$ was confirmed by powder X-ray diffraction (PXRD). For the preparation of composites, the same procedure was used with addition of MgH_2 to the starting mixtures in the following proportions: $3\text{AlCl}_3 + 13\text{LiBH}_4 + 6.5\text{MgH}_2$ and $\text{AlCl}_3 + 4\text{NaBH}_4 + 6.5\text{MgH}_2$. The obtained composites contained mixtures of $\text{Li}_4\text{Al}_3(\text{BH}_4)_{12.74}\text{Cl}_{0.26} + \text{LiCl}$ or $\text{Na}[\text{Al}(\text{BH}_4)_{4-x}\text{Cl}_x] + \text{NaCl}$ with MgH_2 .

Variable-temperature in situ synchrotron PXRD and crystal structure determination

Samples were filled under a high-purity argon atmosphere into 0.5 and 0.7 mm thin-walled glass capillaries. Laboratory diffraction data were obtained with MAR345 diffractometer equipped with a rotating anode ($\text{MoK}\alpha$ radiation) and a XENOCs focusing mirror.

The crystal structure of $\text{Li}[\text{Al}(\text{BH}_4)_4]$ was solved from data collected at varied temperatures at the Materials Science Beamline at PSI (Villigen, Switzerland), using Mythen II detector and $\lambda = 0.775045 \text{ \AA}$.

The temperature was increased linearly in time with $5^{\circ}\text{Cmin}^{-1}$ heating rate. The unit cell was indexed by using FOX,^[52] and the space group $P2_1/c$ was found by ChekCell.^[53] To facilitate the structure solution, the anion $[\text{Al}(\text{BH}_4)_4]^-$ was modeled as a rigid body, using the structural data of $\text{K}[\text{Al}(\text{BH}_4)_4]$. For that, the anion, with 21 atoms, was transformed from the special position in the original $Fddd$ space group to the general position in the $P1$ subgroup by using PowderCell.^[54] The obtained coordinates were transformed into a z-matrix with the program OpenBabel.^[55] Finally, four independent $[\text{Al}(\text{BH}_4)_4]^-$ anions were transferred into FOX and optimized with Li^+ cations. The resulting structure was refined by Rietveld method in Fullprof (Figure S15 in the Supporting Information),^[56] and later validated by DFT calculations (see below).

The crystal structure of $\text{Li}_4\text{Al}_3(\text{BH}_4)_{13}$ was refined using the model of the previously known structure of $\text{Li}_4\text{Al}_3(\text{BH}_4)_{12.74}\text{Cl}_{0.26}$, which contained some chloride atoms on the borohydride sites^[55] (Figure S18 in the Supporting Information).

The crystal structure of $\text{Na}[\text{Al}(\text{BH}_4)_4]$ was solved from in situ synchrotron PXRD data collected at SNBL/ESRF (Grenoble, France) with PILATUS 2 M pixel detector and $\lambda = 0.823065 \text{ \AA}$. The temperature was increased linearly in time at $5^{\circ}\text{Cmin}^{-1}$ rate. The unit cell was indexed and the structure was solved in the space group Cc using FOX.^[48] The final refinement was performed from the synchrotron PXRD data, collected on Materials Science Beamline at PSI (Villigen, Switzerland), using Mythen II detector and $\lambda = 0.775045 \text{ \AA}$. ADDSYM routine in the program PLATON^[57] suggested the $C2/c$ space group. The resulting Rietveld refinement profile was obtained from the DFT-optimized structure, where boron and hydrogen atomic positions, as well as atomic displacement parameters, were refined by full matrix in Fullprof (Figure S19 in the Supporting Information).^[55]

The crystal structures of $\text{NH}_4[\text{Al}(\text{BH}_4)_4]$ and $\text{Rb}[\text{Al}(\text{BH}_4)_4]$ each were solved from in situ synchrotron PXRD data collected at SNBL/ESRF (Grenoble, France) with PILATUS 2 M pixel detector and $\lambda = 0.68884$ and 0.682525 \AA , respectively. Temperature was increased linearly in time using Oxford Cryostream 700+ at a $5^{\circ}\text{Cmin}^{-1}$ heating rate. The 2D images were azimuthally integrated with Bubble software that performs azimuthal integration of raw images.^[58] The unit cells were indexed in the $Fddd$ space group by DICVOL.^[59] The structures were found to be isomorphous to $\text{K}[\text{Al}(\text{BH}_4)_4]$ ^[23] and refined by Rietveld method in Fullprof (Figure S20 and S21 in the Supporting Information)^[55] with the NH_4^+ and BH_4^- groups as semi-rigid tetrahedra with common refined B–H and N–H distances of 1.20 and 1.04 \AA , respectively. No other restraints were used.

The crystal structure of $\text{Cs}[\text{Al}(\text{BH}_4)_4]$ was solved from variable-temperature in situ PXRD data collected at the Materials Science Beamline at PSI (Villigen, Switzerland) by using Mythen II detector and $\lambda = 0.775045 \text{ \AA}$. The temperature was increased linearly in time with $5^{\circ}\text{Cmin}^{-1}$ rate. The unit cell was indexed in the $I4_1/amd$ space group by DICVOL^[58] and the structure was solved in FOX^[51] and refined by the Rietveld method using Fullprof (Figure S22 in the Supporting Information).^[55]

DFT calculations

The structure analysis was performed for all compounds to check and confirm thermodynamic stability and refine positions of the hydrogen atoms. The calculations were performed within periodic plane-wave expansion of the electronic wave functions and density functional theory (DFT) formalism, as implemented in the VASP package.^[60] The electronic configuration of elements was repre-

sented by projected augmented wave^[61] potentials with the following valence states: $1s^1$ for H, $1s^2 2s^1$ for Li, $2s^2 2p^1$ for B, $2s^2 2p^3$ for N, $2p^6 3s^1$ for Na, $3p^6 4s^1$ for K, $4s^2 4p^6 5s^1$ for Rb and $5s^2 5p^6 6s^1$ for Cs. The gradient corrected (GGA) exchange correlation functional was used.^[62]

Static structural optimization was performed with a conjugate gradient method; for each structure the internal atomic positions as well as the lattice parameters were optimized until forces exerted on atoms were smaller than 0.01 eV \AA^{-1} . The experimentally determined configurations were used as starting ones, and the crystal symmetry was constrained during initial structure optimization. Afterwards a simulated annealing search for the possible more stable configuration was performed. This was done by heating the structure to 350 K at a rate of 100 Kps^{-1} and cooling it down to 0 K at a rate of 50 Kps^{-1} . No constraints were imposed on the internal atomic positions and the unit cell parameters were kept fixed during the annealing process. The Nosé-Hoover thermostat^[63] was applied for this procedure and the time step for integration of equations of motion was 0.6 fs. The symmetry of each system was analyzed^[64] after the simulated annealing procedure. Any new symmetry was re-optimized with methods used for the static calculations. For all structures, the normal modes were analyzed. The normal mode frequencies were calculated at the Γ point by displacing the symmetry nonequivalent atoms in each crystallographic direction by $\pm 0.01 \text{ \AA}$.

To compare thermodynamic stability of the mixed-cation compounds at the ground state with respect to the decomposition into $\text{Al}(\text{BH}_4)_3$ and corresponding MBH_4 ($M = \text{Li}^+, \text{Na}^+, \text{K}^+, \text{NH}_4^+, \text{Rb}^+, \text{Cs}^+$), structural optimization and normal mode analysis were performed for all relevant phases. The energy cutoff was increased to 600 eV for the calculations of the ground-state energy. The enthalpy of the reaction was calculated as $\Delta H = E(\text{M}[\text{Al}(\text{BH}_4)_4]) - E(\text{Al}(\text{BH}_4)_3) - E(\text{MBH}_4) + E_0(\text{M}[\text{Al}(\text{BH}_4)_4]) - E_0(\text{Al}(\text{BH}_4)_3) - E_0(\text{MBH}_4)$, where E is the ground-state energy and E_0 is the contribution from zero-point vibrations ($E_0 = \sum h\nu_j/2$).

The Born effective charges Z^* ^[65] were calculated for $\text{M}[\text{Al}(\text{BH}_4)_4]$ ($M = \text{Li}^+, \text{Na}^+, \text{K}^+, \text{Rb}^+, \text{Cs}^+$; Tables S2 and S3 in the Supporting Information). The isotropic component of Z^* is equal to one third of the trace. The ionic radii for cations are based on the data reported by Shannon.^[66]

Acknowledgements

This work was supported by the Académie Universitaire Louvain (AUL, Belgium) under grants ADi/DB/1058.2011 and FNRS (CC 1.5169.12, PDR T.0169.13, EQP U.N038.13). R. Černý acknowledges the support from the Swiss National Science Foundation. We thank ESRF and PSI for the beam time allocation at SNBL and MS beamline at SLS respectively. The research leading to these results received funding from the European Community's Seventh Framework Programme (FP7/2007–2013) under grant agreement no. 312284 (CALIPSO). Z. Łodziana acknowledges CPU time allocation at PLGrid Infrastructure and the support by a grant from Switzerland through the Swiss Contribution to the enlarged European Union.

Conflict of interest

The authors declare no conflict of interest.

Keywords: aluminum • crystal structures • high-energy materials • hydrides • hydrogen storage

- [1] a) M. Paskevicius, L. H. Jepsen, P. Schouwink, R. Černý, D. B. Ravnsbæk, Y. Filinchuk, M. Dornheim, F. Besenbacher, T. R. Jensen, *Chem. Soc. Rev.* **2017**, *46*, 1565–1634; b) R. Mohtadi, A. Remhof, P. Jena, *J. Phys. Condens. Matter* **2016**, *28*, 353001.
- [2] L. E. Klebanoff, J. O. Keller, *Int. J. Hydrogen Energy* **2013**, *38*, 4533–4576.
- [3] A. Züttel, S. Rentsch, P. Fischer, P. Wengera, P. Sudana, Ph. Mauron, Ch. Emmenegger, *J. Alloys Compd.* **2003**, *356–357*, 515–520.
- [4] K. Chłopek, C. Frommen, A. Léon, O. Zabara, M. Fichtner, *J. Mater. Chem.* **2007**, *17*, 3496–3503.
- [5] G. N. Schrauzer, *Naturwissenschaften* **1955**, *42*, 438.
- [6] Y. Nakamori, K. Miwa, A. Ninomiya, H. Li, N. Ohba, S. Towata, A. Züttel, S. Orimo, *Phys. Rev. B* **2006**, *74*, 45126.
- [7] L. H. Rude, T. K. Nielsen, D. B. Ravnsbæk, U. Bösenberg, M. B. Ley, B. Richter, L. M. Arnbjerg, M. Dornheim, Y. Filinchuk, F. Besenbacher, T. R. Jensen, *Phys. Status Solidi A* **2011**, *208*, 1754–1773.
- [8] W. Grochala, P. P. Edwards, *Chem. Rev.* **2004**, *104*, 1283–1315.
- [9] I. Lindemann, R. D. Ferrer, L. Dunsch, Y. Filinchuk, R. Černý, H. Hagemann, V. D'Anna, L. M. L. Daku, L. Schultz, O. Gutfleisch, *Chem. Eur. J.* **2010**, *16*, 8707–8712.
- [10] I. Lindemann, R. D. Ferrer, L. Dunsch, R. Černý, H. Hagemann, V. D'Anna, Y. Filinchuk, L. Schultz, O. Gutfleisch, *Faraday Discuss.* **2011**, *151*, 231–242.
- [11] D. B. Ravnsbæk, Y. Filinchuk, Y. Cerenius, H. J. Jakobsen, F. Besenbacher, J. Skibsted, T. R. Jensen, *Angew. Chem. Int. Ed.* **2009**, *48*, 6659–6663; *Angew. Chem.* **2009**, *121*, 6787–6791.
- [12] D. Ravnsbæk, L. H. Sørensen, Y. Filinchuk, F. Besenbacher, T. R. Jensen, *Angew. Chem. Int. Ed.* **2012**, *51*, 3582–3586; *Angew. Chem.* **2012**, *124*, 3642–3646.
- [13] O. Friedrichs, A. Remhof, A. Borgschulte, F. Buchter, S. I. Orimo, A. Züttel, *Phys. Chem. Chem. Phys.* **2010**, *12*, 10919–10922.
- [14] J. J. Vajo, S. L. Skeith, *J. Phys. Chem. B* **2005**, *109*, 3719–3722.
- [15] J. Graetz, J. J. Reilly, V. A. Yartys, J. P. Maehlen, B. M. Bulychew, V. E. Antono, B. P. Tarasov, I. E. Gabis, *J. Alloys Compd.* **2011**, *509*, S517–S528.
- [16] J. Graetz, B. C. Hauback, *MRS Bull.* **2013**, *38*, 473–479.
- [17] I. Dovgaliuk, Y. Filinchuk, *Int. J. Hydrogen Energy* **2016**, *41*, 15489–15504.
- [18] B. Bogdanović, M. Schwickardi, *J. Alloys Compd.* **1997**, *253–254*, 1–9.
- [19] S. S. Srinivasan, H. W. Brinks, B. C. Hauback, D. Sun, C. M. Jensen, *J. Alloys Compd.* **2004**, *377*, 283–289.
- [20] S.-A. Jin, J.-H. Shim, Y. W. Cho, K.-W. Yi, O. Zabara, M. Fichtner, *Scr. Mater.* **2008**, *58*, 963–965.
- [21] Y. Zhang, Q. Tian, H. Chu, J. Zhang, L. Sun, J. Sun, Z. Wen, *J. Phys. Chem. C* **2009**, *113*, 21964–21969.
- [22] B. R. S. Hansen, D. B. Ravnsbæk, J. Skibsted, T. R. Jensen, *Phys. Chem. Chem. Phys.* **2014**, *16*, 8970–8980.
- [23] I. Dovgaliuk, C. Le Duff, K. Robeyns, M. Devillers, Y. Filinchuk, *Chem. Mater.* **2015**, *27*, 768–777.
- [24] H. I. Schlesinger, R. T. Sanderson, A. B. Burg, *J. Am. Chem. Soc.* **1940**, *62*, 3421–3425.
- [25] a) K. N. Semenenko, O. V. Kravchenko, *Russ. J. Neorg. Chem.* **1972**, *17*, 1084–1086; b) I. Lindemann, A. Borgschulte, E. Callini, A. Züttel, L. Schultz, O. Gutfleisch, *Int. J. Hydrogen Energy* **2013**, *38*, 2790–2795.
- [26] D. A. Knight, R. Zidan, R. Lascola, R. Mohtadi, C. Ling, P. Sivasubramanian, J. A. Kaduk, S.-J. Hwang, D. Samanta, P. Jena, *J. Phys. Chem. C* **2013**, *117*, 19905–19915.
- [27] P. Sims, T. Aoki, R. Favaro, P. Wallace, A. White, C. Xu, J. Menendez, J. Kouvetakis, *Chem. Mater.* **2015**, *27*, 3030–3039.
- [28] S. Schneider, T. Hawkins, Y. Ahmed, M. R. L. Hudgens, J. Mills, *Angew. Chem. Int. Ed.* **2011**, *50*, 5886–5888; *Angew. Chem.* **2011**, *123*, 6008–6010.

- [29] I. Dovgaliuk, V. Ban, Y. Sadikin, R. Černý, L. Aranda, N. Casati, M. Devillers, Y. Filinchuk, *J. Phys. Chem. C* **2014**, *118*, 145–153.
- [30] P. Schouwink, B. M. Ley, A. Tissot, H. Hagemann, T. R. Jensen, L. Smrčok, R. Černý, *Nat. Commun.* **2014**, *5*, 5706.
- [31] P. Schouwink, F. Morelle, Y. Sadikin, Y. Filinchuk, R. Černý, *Energies* **2015**, *8*, 8286–8299.
- [32] A. J. Downs, L. A. Jones, *Polyhedron* **1994**, *13*, 2401–2415.
- [33] J.-Ph. Soulié, G. Renaudin, R. Černý, K. Yvon, *J. Alloys Compd.* **2002**, *346*, 200–205.
- [34] V. A. Blatov, *Struct. Chem.* **2012**, *23*, 955–963.
- [35] a) J. M. Newsam, A. K. Cheetham, B. C. Tofield, *Solid State Ionics* **1980**, *1*, 377–393; b) R. W. G. Wyckoff, *Z. Kristallogr.* **1925**, *62*, 529–539.
- [36] Y. Filinchuk, D. Chernyshov, V. Dmitriev, *Z. Kristallogr.* **2008**, *223*, 649–659.
- [37] R. Černý, G. Severa, D. B. Ravnsbæk, Y. Filinchuk, V. D'Anna, H. Hagemann, D. Haase, G. M. Jensen, T. R. Jensen, *J. Phys. Chem. C* **2010**, *114*, 1357–1364.
- [38] M. E. Bowden, G. J. Gainsford, W. T. Robinson, *Aust. J. Chem.* **2007**, *60*, 149–153.
- [39] R. Flacau, C. I. Ratcliffe, S. Desgreniers, Y. Yao, D. D. Klug, P. Pallister, I. L. Moudrakovski, J. A. Ripmeester, *Chem. Commun.* **2010**, *46*, 9164–9166.
- [40] L. G. Sillén, A. L. Nylander, *Ark. Kemi Mineral. Geol.* **1943**, *17A*, 1–27.
- [41] T. Jaroń, W. Wegner, W. Grochala, *Dalton Trans.* **2013**, *42*, 6886–6893.
- [42] M. P. Kokkoros, *Prakt. Athener Akad.* **1942**, *17*, 163–174.
- [43] T. J. Marks, J. R. Kolb, *Chem. Rev.* **1977**, *77*, 263–293.
- [44] S. Aldridge, A. J. Blake, A. J. Downs, R. O. Gould, S. Parsons, C. R. Pulham, *J. Chem. Soc. Dalton Trans.* **1997**, 1007–1012.
- [45] P. Błoński, Z. Łodziana, *Phys. Rev. B* **2014**, *90*, 054114.
- [46] M. Gutowski, T. Autrey, *Prepr. Pap. - Am. Chem. Soc. Div. Fuel Chem.* **2004**, *49*, 275–276.
- [47] L. Pauling, *J. Am. Chem. Soc.* **1929**, *51*, 1010–1026.
- [48] L. H. Jepsen, M. B. Ley, Y. Su-Lee, Y. W. Cho, M. Dornheim, J. O. Jensen, Y. Filinchuk, J. E. Jørgensen, F. Besenbacher, T. R. Jensen, *Mater. Today* **2014**, *17*, 129–135.
- [49] C. J. Wen, B. A. Boukamp, R. A. Huggin, *J. Electrochem. Soc.* **1979**, *126*, 2258–2266.
- [50] G. Balducci, S. Brutti, A. Ciccio, G. Gigli, P. Manfrinetti, A. Palenzona, M. F. Butman, L. Kudin, *J. Phys. Chem. Solids* **2005**, *66*, 292–297.
- [51] R. W. Parry, D. R. Schultz, P. R. Girardot, *J. Am. Chem. Soc.* **1958**, *80*, 1–3.
- [52] V. Favre-Nicolin, R. Černý, *J. Appl. Crystallogr.* **2002**, *35*, 734–743.
- [53] LMGP-Suite Suite of Programs for the interpretation of X-ray Experiments, by Jean laugier and Bernard Bochu, ENSP/Laboratoire des Matériaux et du Génie Physique, BP 46. 38042 Saint Martin d'Hères, France. WWW: <http://www.inpg.fr/LMGP> and <http://www.ccp14.ac.uk/tutorial/lmgp/>.
- [54] W. Kraus, G. Nolze, *J. Appl. Crystallogr.* **1996**, *29*, 301–303.
- [55] N. M. O'Boyle, M. Banck, C. A. James, C. Morley, T. Vandermeersch, G. R. Hutchison, *J. Cheminf.* **2011**, *3*, 33.
- [56] J. Rodríguez-Carvajal, *Physica B* **1993**, *192*, 55–69.
- [57] A. L. Spek, PLATON. University of Utrecht, The Netherlands, **2006**.
- [58] V. Dyadkin, P. Pattison, V. Dmitriev, D. Chernyshov, *J. Synchrotron Radiat.* **2016**, *23*, 825–829.
- [59] J. Rodríguez-Carvajal, *Physica B* **1993**, *192*, 55–69.
- [60] G. Kresse, J. Furthmüller, *Phys. Rev. B* **1996**, *54*, 11169.
- [61] P. E. Blöchl, *Phys. Rev. B* **1994**, *50*, 17953.
- [62] J. P. Perdew, K. Burke, M. Ernzerhof, *Phys. Rev. Lett.* **1996**, *77*, 3865.
- [63] S. Nosé, *J. Chem. Phys.* **1984**, *81*, 511–519.
- [64] H. T. Stokes, D. M. Hatch, *J. Appl. Crystallogr.* **2005**, *38*, 237–238.
- [65] M. Born, K. Huang, *Dynamical Theory of Crystal Lattices*, Oxford University Press, Oxford, UK, **1954**.
- [66] R. D. Shannon, *Acta Crystallogr. Sect. A* **1976**, *32*, 751–767.

Manuscript received: August 27, 2017

Revised manuscript received: October 4, 2017

Accepted manuscript online: October 5, 2017

Version of record online: November 22, 2017